Received: 30 April 2020 | Revised: 15 September 2020 | Accepted: 12 October 2020

DOI: 10.1002/prot.26016

RESEARCH ARTICLE

PROTEINS WILEY

Tuning the binding interface between Machupo virus glycoprotein and human transferrin receptor

Dick J Sjöström[1] | Anneli Lundgren[1] | Scott J Garforth[2] | Sinisa Bjelic[1]

[1]Department of Chemistry and Biomedical Sciences, Linnaeus University, Kalmar, Sweden

[2]Department of Biochemistry, Albert Einstein College of Medicine, New York, New York

Correspondence
Sinisa Bjelic, Department of Chemistry and Biomedical Sciences, Linnaeus University, Stuvaregatan 2, 392 31 Kalmar, Sweden.
Email: sinisa.bjelic@lnu.se

Funding information
Faculty of Health and Life Sciences, Linnaeus University; VINNOVA, Grant/Award Number: 2015-04912

Abstract

Machupo virus, known to cause hemorrhagic fevers, enters human cells via binding with its envelope glycoprotein to transferrin receptor 1 (TfR). Similarly, the receptor interactions have been explored in biotechnological applications as a molecular system to ferry therapeutics across the cellular membranes and through the impenetrable blood–brain barrier that effectively blocks any such delivery into the brain. Study of the experimental structure of Machupo virus glycoprotein 1 (MGP1) in complex with TfR and glycoprotein sequence homology has identified some residues at the interface that influence binding. There are, however, no studies that have attempted to optimize the binding potential between MGP1 and TfR. In pursuits for finding therapeutic solutions for the New World arenaviruses, and to gain a greater understanding of MGP1 interactions with TfR, it is crucial to understand the structure–sequence relationship driving the interface formation. By displaying MGP1 on yeast surface we have examined the contributions of individual residues to the binding of solubilized ectodomain of TfR. We identified MGP1 binding hot spot residues, assessed the importance of posttranslational *N*-glycan modifications, and used a selection with random mutagenesis for affinity maturation. We show that the optimized MGP1 variants can bind more strongly to TfR than the native MGP1, and there is an MGP1 sequence that retains binding in the absence of glycosylation, but with the addition of further amino acid substitutions. The engineered variants can be used to probe cellular internalization or the blood-brain barrier crossing to achieve greater understanding of TfR mediated internalization.

KEYWORDS

blood-brain barrier, flow cytometry, fluorescence-activated cell sorting, Machupo virus glycoprotein 1, Rosetta, transferrin receptor, yeast surface display

1 | INTRODUCTION

Transferrin receptor (TfR) together with iron transporter protein transferrin (Tf) is responsible for iron homeostasis in human cells.[1,2]

Abbreviations: BBB, blood-brain barrier; H-Ft, H-Ferritin; HFE, hemochromatosis protein; MGP1, Machupo virus glycoprotein 1; *Pv*RBP2b, *P. vivax* reticulocyte-binding protein b2; SAPE, Streptavidin–R-Phycoerythrin Conjugate; Tf, transferrin; TfR, transferrin receptor 1; YSD, yeast surface display.

Iron insolubility and reactivity has made it necessary to dedicate a specific transport system, leading to ubiquitous expression of Tf in blood and TfR on the surface of the cells. Upon interface formation between Tf and TfR, the complex is internalized, leading to iron release from Tf and shuttling of the components back into blood for the next round of iron delivery. Besides the iron carrier, Tf, the receptor also interacts with another iron carrier protein, H-Ferritin (H-Ft),[3] hereditary hemochromatosis protein (HFE),[4,5] malaria parasite *Plasmodium vivax* reticulocyte-binding protein b2 (PvRBP2b),[6] and with the envelope glycoproteins of clade B New World *Arenaviridae* viruses, that exploit TfR for cell entry. To date, studies of several such arenaviruses (Machupo, Junín, Guanarito, Sabiá, and Chapare) have identified genetically conserved residues in envelope glycoproteins and assessed some of their interactions with TfR.[7-10] Tf and HFE binding, on the other hand, has been well studied with the respect to the mutations at the interface,[11-13] and the structures of several complexes have been determined.[4,14] In these structures, the ectodomain of the TfR is a symmetrical homodimer each composed of apical, protease-like, and helical domains; Tf and HFE proteins bind mainly to the helical domain, with HFE being a binding competitor of Tf.[12,13] The viruses, on the contrary, form interactions at the apical domain with their glycoprotein, and thus share the binding domain with H-Ft and *Pv*RBP2b.[15]

An exciting aspect of the iron delivery system has been its utilization for drug delivery into cells and the long-sought transport across the blood–brain barrier (BBB) into the central nervous system.[16] To this end several delivery strategies have been devised, among others, antibodies against TfR coupled with protein therapeutics to target β-amyloids and β-secretase enzyme (BACE1); such TfR antibodies localize in the brain in an effort to maximize the drug efficacy.[17] The molecular details of interaction between these antibodies and TfR are not known. It has been suggested that Tf undergoes transcytosis that shuttles the complex across the endothelial cells of the BBB. The strength of the binding interaction for the complex formation with TfR has been implied to be important for endocytosis and transcytosis where stronger binding may not lead to higher level of localization in biological compartments but to degradation of the internalized complex.[18] This is in direct contrast to the general principles behind therapeutic protein-protein complex formation where high selectivity is required to avoid off-target effects. In addition, other avenues of molecular interaction to TfR have been previously developed: short peptides,[19] TfR targeting scFV fused to therapeutics, and gold nanoparticles coated with Tf[20] or coupled with anti TfR specific antibodies.[18] Since there is no evidence that clade B New World viruses use the mechanism of transcytosis to cross the BBB, or that they are able to significantly localize into the brain, it would be highly interesting to provide answers to such questions. Ability to modulate the binding strength of the viral glycoproteins to TfR, and especially to gain a better understanding of structure–sequence relationships, would lay groundwork for future studies of the passage through the BBB.

The fate of the formed complex with TfR, whether by endogenous or exogenous partners, is internalization by cells. In the case of Tf, when two iron-bearing proteins are bound to the dimeric TfR they are endocytosed, after which bound iron is released in the endosomal acidic environment.[14] It is likely that the viruses enter cells by similar mechanisms. However, mechanistic details are lacking of how complex formation of proteins other than Tf with TfR leads to different checkpoint decisions discriminating between disparate fates of cell internalization vs tagging for proteasomal degradation. It would be beneficial to gain thorough understanding of such mechanisms not only for understanding the biological processes, but also for more successful biotechnological applications.

To learn more about the complex formation between Machupo virus glycoprotein 1 (MGP1) and TfR we have optimized their molecular interactions. We focused on the previously published complex of Machupo arenavirus glycoprotein co-crystallized with the receptor, MGP1–TfR (PDB ID: **3kas**[21]), which facilitates the analysis of mutational data in the context of the determined structure. To experimentally investigate MGP1 binding to TfR we displayed the virus protein on the yeast surface, and monitored binding with flow cytometry. The assay has been combined with single-residue mutagenesis to assess the binding interface based on the predicted hot spot residues, redesign of posttranslationally modified sites, and selection assay. Furthermore, we evaluated the interface formation by engineering an MGP1 variant, that was shown to bind TfR by yeast surface display (YSD).[22,23] Since TfR is biologically relevant and a promising target for transporting protein therapeutics into cells and across the BBB, greater understanding of the MGP1–TfR interface formation constitutes a valuable starting point for investigation of complex internalization without disrupting the Tf–TfR mediated iron transport mechanism.[18]

2 | MATERIALS AND METHODS

2.1 | Cloning and plasmid purification

The genes encoding for the native MGP1 (residues 84-244, Figure S1), single mutants I115A, V117A, N95A, N137A, N166A, and N178A, and the combined N95D/I126V/E130D/N137A/N166A/K170M/N178D variant were ordered from IDT (Integrated DNA Technologies). The linear pETCON[24] plasmid, cleaved with FastDigest NdeI and XhoI (Thermo Scientific) and a corresponding gene were used to construct the expression vectors by homologous recombination in *Saccharomyces cerevisiae* EBY100 strain. The cloning was confirmed by sequencing after colony PCR. Each colony was dissolved in 20 μL reactions containing 5 mg/mL zymolase (Seikagaku corporation, Japan), 250 mM HEPES, 2 M sorbitol, and 15% glycerol, pH 7.4 and incubated for 1 hour at 37°C in adaptation of protocol from Singh et al. [25]. Two microliter of the zymolase reaction was subjected to 30 PCR amplification cycles with the forward and reverse primers: CCATACGACGTTCCAGACTACG and CTATTACAAGTCCTCTTCAGAA. After PCR cleanup with ExoSAP-IT (Thermo Fisher Scientific), one of the primers was added to the Mix2Seq kit (EuroFins, Germany) for sequencing. For plasmid purification, cells were lysed with zymolase, from 10 mL of yeast cells, grown ON to an

OD_{600} = 6 in C–UT growth medium. C–UT medium was prepared as follows: 1.85 g/L synthetic complete mixture, Kaiser, drop-out–*Trp*–*Ura* (Formedium, England), 6.9 g/L yeast nitrogen base without amino acids with ammonium sulfate (Formedium, England), and 20 g/L d-(+)-glucose (Sigma-Aldrich). QIAprep spin Miniprep Kit (Qiagen, Germany) was used to extract the plasmid.

2.2 | Construction of MGP1 mutagenesis library

pETCON containing MGP1 was used for random mutagenesis (MutazymeII kit, Stratagene) with the sequencing primers to generate the library of MGP1 variants. Two reactions were set up with 5 and 500 ng MGP1 to titrate the optimal number of mutations per gene. Both PCR reactions were transformed into yeast by electroporation in 0.2 cm cuvettes (Bio-Rad) at 2.5 kV, with 1 μg pETCON, 3 μg MGP1, conditioning with 0.1 M LiAc (Sigma-Aldrich), and 10 mM DTT (Fisher Bioreagents), in a volume of 100 μL following the published protocol.[26] The electroporated cells were transferred into 10 mL of a 1:1 mix of 2 M sorbitol and YPD medium (20 g/L peptone (Nordic biolabs, Sweden), 10 g/L yeast extract [Sigma-Aldrich], 20 g/L d-(+)-glucose [Sigma-Aldrich]), and incubated shaking at 30°C for 1 hour. The cells were collected and resuspended in 50 mL C–UT medium, and the number of transformants was determined by plating 5 μL and 50 μL of the culture on selective C–UT agar plates, respectively. After incubation a 30°C for 2 days, colony-forming units were counted to calculate the size of the mutagenesis library. Errors per gene were determined based on the DNA sequencing with Mix2Seq kit (EuroFins, Germany).

2.3 | Fluorescence-activated cell sorting of MGP1 library

YSD method, developed by Wittrup lab,[27] had been used to assay binding of MGP1 and variants thereof with TfR. During YSD we determined both MGP1 protein expression and binding to the receptor target by quantifying the increase of the respective fluorescence signal by bound conjugate proteins. In brief, EBY100 yeast cells were passaged overnight in C–UT medium to an OD_{600} 5 to 6, before the protein surface expression was induced by switching to C–UT medium containing galactose instead of glucose with OD_{600} = 0.75, incubated at 20°C with 200 rpm shaking for 24 hours. Five hundred microliter induced cells were washed with 1 mL PBSF (8 g NaCl, 0.2 g KCl, 1.44 g Na_2HPO_4, 0.24 g KH_2PO_4, and 1 g bovine serum albumin in 1 L deionized sterile filtered H_2O, adjusted to pH 7.4), thereafter labeled on ice for 1.5 hours at 1 μM TfR, filled up to 500 μL with PBSF. With samples kept on ice until measurement, another wash with 1 mL PBSF was performed before 30 minutes of labeling with 1:100 diluted chicken anti-cmyc-FITC conjugated antibody that monitored yeast surface protein expression (Immunology Consultants Laboratory) and 1:18.9 SAPE (Streptavidin-R-Phycoerythrin Conjugate; Invitrogen) that detected biotinylated TfR binding to yeast expressed protein, reaching a total volume of 500 μL with PBSF. The cells were washed with PBSF, pelleted, and kept on ice until sorting with a BD Influx. SAPE was excited with a yellow-green laser (561 nm) and FITC with a blue laser (488 nm). The bandpass filters used to detect SAPE and FITC were 585/29 and 530/40, respectively. Cells were resuspended in PBSF, gated on the top 5% in the first sort and top 1% of cells in subsequent rounds of FACS. The first two sorts were carried out after incubation with 1 μM TfR, while in the last three sorts the labeling was done at 0.1 μM TfR. Cells were collected in C–UT supplemented with penicillin and streptomycin. Between each round of FACS, the cells were passaged twice in 50 mL C–UT medium. During the YSD assay control experiments were always carried out in parallel with anti-cmyc-FITC conjugated antibody and SAPE present, but without target TfR added. These negative control experiments resulted in complete loss of binding signal.

2.4 | TfR expression and purification

The sequence encoding amino acids 121 to 760 of hTFR was cloned into a derivative of the pIRES-GFP vector (Clontech), under a CMV promoter. The native signal peptide was replaced with the human EPO signal peptide, and the protein was engineered to contain a C-terminal BirA recognition sequence, TEV recognition sequence, and 10xHis sequence. Five hundred milliliters HEK 293F in FreeStyle media (Life Technologies) were transfected with the expression plasmid using PEI.[28] Twenty-four hours post-transfection VPA was added in 100 mL FreeStyle media to a final volume of 3 mM. Culture supernatant was harvested 8 days post transfection by centrifugation at 4000*g* for 10 minutes, and AEBSF and imidazole added to the culture supernatant to final concentrations of 0.2 and 5 mM, respectively. Twelve milliliters of a 50% slurry of nickel-IDA (His60, Takara) was added, and stirred at 4°C for 1 hour. Resin was poured into a disposable plastic chromatography column (Bio-Rad, EconoPrep), washed with five bed volumes wash buffer (20 mM HEPES, pH 7.6, 500 mM NaCl, 5 mM imidazole, 10% glycerol), and eluted with the same buffer containing 500 mM imidazole. Fractions enriched for hTFR protein were pooled and purified by gel filtration chromatography (HiLoad 16/60 Superdex 200) in 20 mM HEPES, pH 7.6, 250 mM potassium glutamate, 10% glycerol. Protein was concentrated to 0.8 mg/mL, and snap frozen. Additional C-terminal residues that were added included the BirA recognition sequence and the TEV protease cleavage site as follows: GSGLNDIFEAQK IEWHEGGGSENLYFQSGGSHHHHHHHHHH. Biotinylation of TfR with BirA (Avidity) was done for 40 minutes at 30°C at a TfR concentration of 19.2 μM in 20 mM HEPES, 250 mM HKGlu, pH 7.6, with 8 parts TfR, 1 part biomix A, 1 part biomix B, and 2.5 μg BirA per 10 nmol TfR. Excess biotin was removed by gel filtration (Superdex 200 HR 10/30) in 20 mM HEPES, 150 mM NaCl, 10% glycerol, pH 7.6.

2.5 | Flow cytometry analysis of yeast displayed variants

Preparation of protein expressing yeast was performed as described for FACS of the MGP1 library. Labeling was done by scaling down

10 times the number of cells and used volumes, but following the same incubation protocol. For competition assay, labeling was carried out at 100 nM biotinylated TfR in the presence of 1 μM unlabeled TfR. Two independent measurements were done, one with a BD Accuri C6 flow cytometer, and one with a Bio-Rad S3e cell sorter. Both use a blue (488 nm) laser and the bandpass filters for detecting FITC and SAPE, respectively, were 533/30 and 585/40 for the BD Accuri C6 and 525/30 and 586/25 for S3e. Flow cytometry figures were prepared with FlowJo software.[29] Flow cytometry controls of unlabeled yeast population, and individually labeled by FITC or SAPE showed no unspecific binding (c.f. supplementary information section).

2.6 | Apparent binding affinity determination

Apparent dissociation constant, K_d, was determined by titrating TfR from 0.002 nM to 10 000 nM.[27] The measurement of binding signal was carried out with a BD Accuri C6 flow cytometer at 12 concentrations around an estimated apparent K_d, with a factor of 3.3 between each adjacent point. All values were determined in triplicates. Each sample consisted of 50 μL induced cells of OD_{600} = 0.75, labeled as described previously with volumes linearly adjusted.[27] The fitting and apparent K_d was calculated using R[30] and the Dose Response Curve package.[31]

2.7 | Computational modeling of MGP1-TfR interface

RosettaScripts application[32] of Rosetta protein modeling software[33] was used to optimize the binding interface between TfR and MGP1 (protocol executed according to the supplementary information). Backbone and side-chain optimization of torsional angles was used to generate local minima structures for local, rigid-body perturbations of the binding partners (PDB ID: **3kas**[21]). This was followed by additional optimization of side chains. In total 100 structures were generated to calculate the residue contribution to the binding interface formation according to the implemented "ddG" mover. RosettaRemodel[34] was used with a blueprint file, allowing mutation to 20 naturally occurring amino acids at position 178, and the relaxed PDB structure **3kas** was used to determine the most favorable substitutions of Asn^{178}. In both applications Rosetta energy function Ref2015 has been used.[35] All molecular graphics work has been prepared by PyMol.[36]

2.8 | PSSM construction of MGP1

The PSSM for MGP1, in the PDB structure **3kas**, was generated with PSIBLAST[37-39] (version 2.2.31+) with two iterations and an e-value threshold of 0.0009. The Kullback-Leibler logo sequence in Figure S2 was made with seq2logo.[40]

3 | RESULTS

We have investigated the molecular details of MGP1-TfR interface formation by introducing single point mutations into MGP1 gene sequence (Figure S1) and by randomly searching the protein sequence space for functional variants with the help of the selection. We have found novel variants of MGP1 that modulate binding to TfR according to the yeast display binding assay. The experimental results from assessed mutants led to a combined variant that is free of post-translational modifications, but in which the binding is similar to the native protein.

3.1 | Probing the MGP1-TfR interface formation

To investigate the energetic contribution of individual residues to the interface formation we have carried out structural modeling with Rosetta protein modeling software which allows us to locally perturb the complex and optimize side chains binding interactions with the surrounding. The favorable positions of MGP1 were then substituted with alanine and assessed experimentally for binding by YSD.

The computational part was based on the previously defined five unique interaction motifs that constitute the interaction surface of MGP1 and TfR[21]; we have chosen representative residues in these motifs and calculated their contribution to complex formation (Figure 1A). Several residues were predicted to be important in binding of MGP1 to TfR, including Ile^{115}, which has the lowest interaction energy, followed by Val^{117} and Phe^{226}. Ile^{115} and Val^{117} are both next to the aromatic ring of the central residue, Tyr^{211}, on the interaction surface of TfR (Figure 1B).

Since the isoleucine and valine residues are in the same interaction motif, and from visual inspection form substantial contacts, they have been experimentally tested by YSD. The experimental strategy allows us to test variants with respect to both protein expression and binding to the target. Thus, yeast surface expression of tested variants was monitored by increase of the anti-cmyc antibody-FITC signal when bound to the C-terminally presented myc tag. The interaction of the displayed protein with the TfR was similarly measured by streptavidin (SA) conjugated phycoerythrin (PE) fluorescence following the incubation with the biotinylated receptor. Yeast fluorescence was subsequently quantified on a flow cytometer and analyzed by flow cytometry plots where displayed protein variants that bound TfR showed a population toward upper, right quadrant (Figure 1C).

In agreement with the computational prediction, each alanine variant greatly reduced the formation of the complex. These showed almost completely diminished binding at high concentration (10 μM) TfR (Figure 1C). Thus, two likely hot spot residues Ile^{115} and Val^{117}, contribute substantially to MGP1–TfR interface formation.

The interface is furthermore formed by glycans as MGP1 protein is heavily glycosylated on four asparagine residues; the glycans are in direct contact with the TfR residues (4-5 Å) in all cases, but for Asn^{137} (∼11 Å), as determined by distance measurements within the

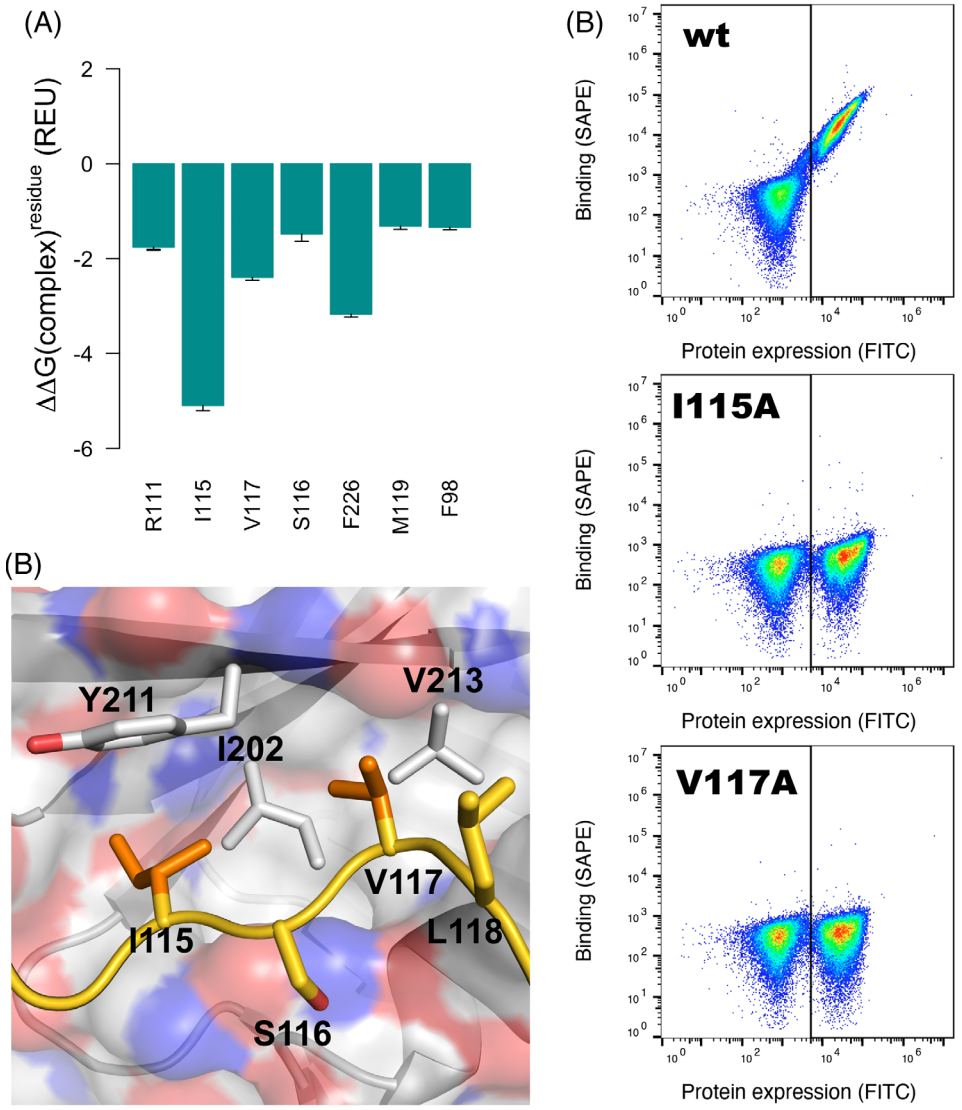

FIGURE 1 Identification of MGP1 hot spot residues. A, Computationally predicted residue contributions to the MGP1 complex formation with TfR (REU, Rosetta energy units). Average values presented with error bars at one SD calculated over 100 trajectories. B, The hydrophobic interface between the interface hot spots Ile^{115} and Val^{117} of MGP1 and Tyr^{211}, Ile^{202}, and Val^{213} on the receptor. C, Flow cytometry data of yeast surface displayed wild type MGP1 as well as Ile^{115} and Val^{117} alanine mutants. 50 000 gated singlet cells were measured at 10 μM TfR. Cells expressing MGP1 were detected with anti-cmyc antibody conjugated with FITC (abscissa), and were gated on the right side of the middle black line. The biotinylated TfR binding signal to MGP1 was detected with SAPE (ordinate). The I115A and V117A variants do not bind TfR establishing these positions as the hot spot residues (the binding signal drops from MFU 20 000 for wt to less than 300 for the alanine mutants)

MPG1-TfR complex (PDB ID: **3kas** [21]). These glycans differ in the extent of interactions with the TfR depending on their branching and distances from the receptor. The branching makes it possible to reach the receptor, for example, the first modified site in the protein sequence, Asn^{95}, is situated about 9 Å above the backbone of TfR Gly^{207} while the next residues, Asn^{137}, is ∼14 Å from Gln^{187}. Asn^{166} is the closest residue to the interface with only ∼7 Å between its side chain and TfR Glu^{294}. The last glycosylation site on Asn^{178}, situated in a pocket of MGP1 formed mainly by several loops, is 10 Å from TfR Gly^{347}. Out of the four glycosylated positions, Asn^{95} and Asn^{178} are conserved within arenaviruses (Figure S2, according to the published data [21,41]) To investigate the impact of MGP1 glycosylation sites (Figure 2A) on complex formation with TfR, we mutated the post-translationally modified residues to alanine (Figure 2B). Mutation of the glycosylation sites resulted in approximately native TfR binding for the N137A and N166A variants, while N95A lost 80% of the binding signal and for N178A the binding signal dropped to the background levels (Figure 2B and Table S1). Our measurements agree with the evolutionary data, as can be seen from the multiple sequence alignment for the MGP1 in which the glycosylated positions Asn^{95} and Asn^{178} are conserved (Figure S2).

3.2 | Optimization of MGP1-TfR binding by YSD/FACS

To carry out affinity maturation of MGP1 for improved binding to TfR we have used FACS of the yeast displayed variants. On average the library consisted of about 10^5 variants with ∼1 mutation per MGP1 gene (Table S2). After five rounds of FACS, three MGP1 variants were identified with improved binding to TfR when compared to the native MGP1 (Figure 3A,B, Table S2). The mean fluorescent signal, measured at 100 nM TfR, increased up to the third sort, decreased after a fourth sort, and increased once again for the fifth sort (Figure 3B and Table S1). The sequencing revealed two mutants from sort 3 and one from sort 5 with a distinctly strong mean fluorescent signal compared

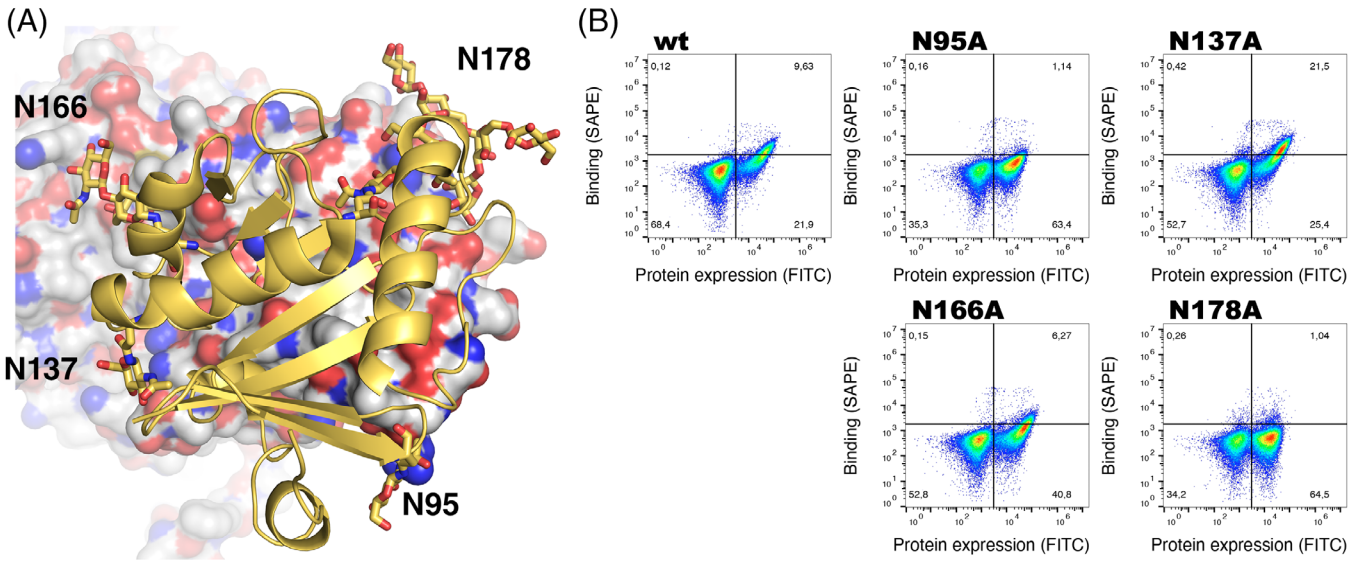

FIGURE 2 Alanine scan of glycosylation sites in MGP1. A, Top view of MGP1 (yellow) bound to TfR (gray), with the four *N*-glycosylated residues shown as sticks. B, Flow cytometry binding data of yeast displayed MGP1 variants where each of the posttranslationally modified residues were mutated to alanine. Assay carried out at 1 μM TfR for 60 000 cells gated for singlets, and in each quadrant the percentage of cells is indicated. The four variants tested were all expressed on yeast surface as measured by FITC labeling (abscissa), and only the N178A mutation abolished binding as detected by SAPE labeled TfR (ordinate) [Color figure can be viewed at wileyonlinelibrary.com]

with wild type (Figure 3C). N95D/G230D and N95D/I126V/E130D/K170M variants were found in sort 3 while L94P/F98L/H204R/G230D was found in sort 5. The sequencing from sort 3 revealed that the library converged to variants containing the N95D mutation (7/8 sequenced variants); continued sorting for 2 additional rounds elicited the L94P/F98L/H204R/G230D (3 out of 8 sequenced variants). In the last sort we found another variant (N150D/K170M/E209K/G230D), but it did not bind TfR better than the N95D containing mutants from sort 3. The change in the resulting variants between sorts 3 and 5 can be due to the presence of distinct populations in sort 4 that drive the screen toward different sequence spaces. All sequencing data, obtained from different sorts, is presented in Table S2.

The double mutant variant MGP1.b1 (MGP1 N95D/G230D) was further studied as it had fewer mutations and similar binding signal compared to the variants with four mutations each. The N95D variant had the largest contribution to the increased binding, ∼90% retained signal, compared to the double mutant, and G230D did heighten the signal slightly when combined with Asp^{95}, measured at 100 nM TfR (Figure S3). The competition assay of yeast displayed *b1* variant with 10-fold excess of unlabeled:labeled TfR eliminated the binding signal by 80%, demonstrating specific interaction to TfR. The apparent dissociation binding constant, K_d, was determined to be 1.5 ± 0.18 μM for MGP1 and 47 ± 4 nM for MGP1.b1 according to the sigmoidal curve fit to the flow cytometry data (Figure 3D); the MGP1.b1 variant showed thus about 30 times improved apparent binding affinity compared with the native as determined by yeast display. There are currently no other published data for the TfR–MGP1 K_d for comparison. Interestingly, from the investigation of glycosylation effects on binding, evidence was found that posttranslationally modified Asn^{95} had an important contribution to interface formation, however, the iterative screening of the random library provided an alternative answer with an aspartic acid at the corresponding position improving binding. Although, when compared to N178A mutant, N95A did show some weak tendencies toward complex formation (N95A exhibited ∼20% binding signal vs the native, Table S1) indicating that this position may be more susceptible to optimization.

3.3 | Engineering the glycan free MGP1 variant

Next, we combined the mutations found during the affinity maturation with those that abolish the posttranslationally glycosylated sites. Since N178A glycosylation knockout seems to disrupt the binding signal completely (Figure 2B), unglycosylated Asn^{178} was computationally evaluated for alternative residues that theoretically could conserve binding to TfR similarly to the Asn^{95} position where N95D improved binding. N178D was computationally identified as a substitution that could potentially retain binding while abolishing the glycosylation site, and was incorporated into a new variant that consisted in total of seven mutations, MGP1.c1 (N95D/I126V/E130D/N137A/N166A/K170M/N178D). This combined variant bound TfR at 1 μM concentration with lower affinity, ∼40%, when compared to the native MGP1 (Figure 4, Table S1, variants in Figures 2 and 4 were assayed at the same time) showing thus a binding signal relative to the unproductive complex formation between MGP1 N178A and TfR. Further sorting of a randomized MGP1.c1 variant by FACS lead unfortunately to fast emergence of a reverting D178N mutation.

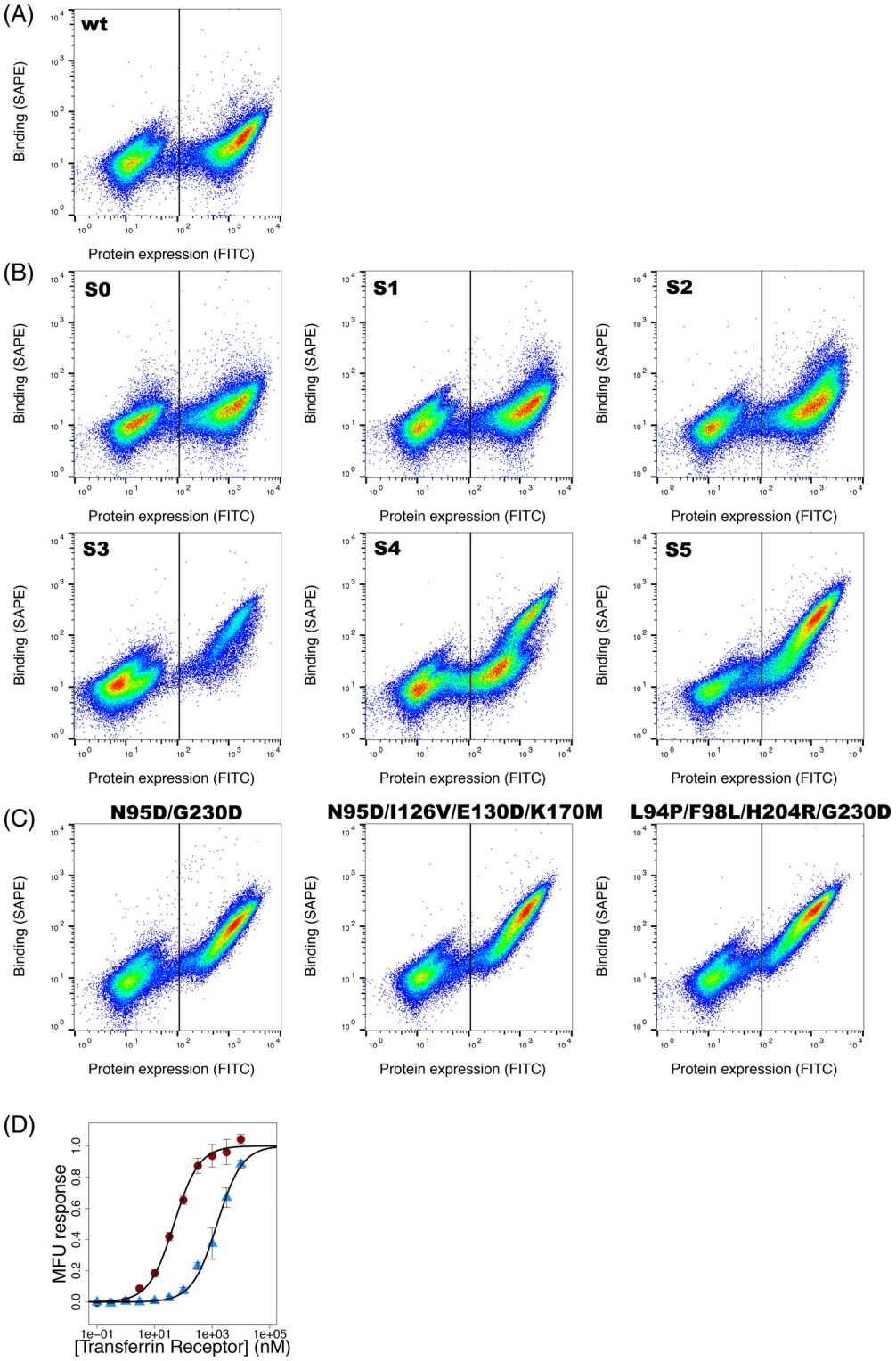

FIGURE 3 MGP1 selection and evaluation of improved variants. Flow cytometry of yeast displayed variants measured for 50 000 gated singlet cells per sample at 100 nM TfR. A, Wild type MGP1. B, Sorted MGP1 library (s0-5 indicate sort 0-5). During FACS the MGP1 library was narrowed to three variants, by selecting the top 3% to 5% in the first two rounds of sorting, thereafter the top 1% of the binding variants. Sorting was carried out after labeling at 1 μM TfR (sort 1-2), thereafter at 100 nM. C, The N95D/G230D and N95D/I126V/E130D/K170M mutations were identified in the third sort and in the fifth sort the third MGP1 mutant was identified. **d)** Triplicates of flow cytometry measurements of 50 000 cells per sample and TfR concentration. MGP1 native (triangles) and the evolved N95D/G230D variant (filled circles) resulted in apparent $K_{d,}^{native}$ = 1.5 ± 0.18 μM and $K_d^{N95D/G230D}$ = 47 ± 4 nM, respectively. Bars indicate one SD [Color figure can be viewed at wileyonlinelibrary.com]

4 | DISCUSSION

TfR is responsible for delivery of protein-bound iron into cells and has been one of the most explored mechanism of cargo delivery into cells and across the BBB.[16] Short peptides, 7 and 12 amino acids long found by phage display, bind TfR and enter receptor expressing cells.[19] Fusing a potentially therapeutic antibody to TfR targeting scFV has been shown to increase transport across the BBB in mice comparable to small molecule levels of brain uptake.[42] In another method, traversing of the BBB was explored by using gold nanoparticles coated with Tf which have been shown to cross the mouse BBB, by taking advantage of avidity, that the approach provides.[20] In these studies, the coated Tf has to compete with Tf present in the blood, which is at a concentration of ~38 μM,[43] and in diferric form has an

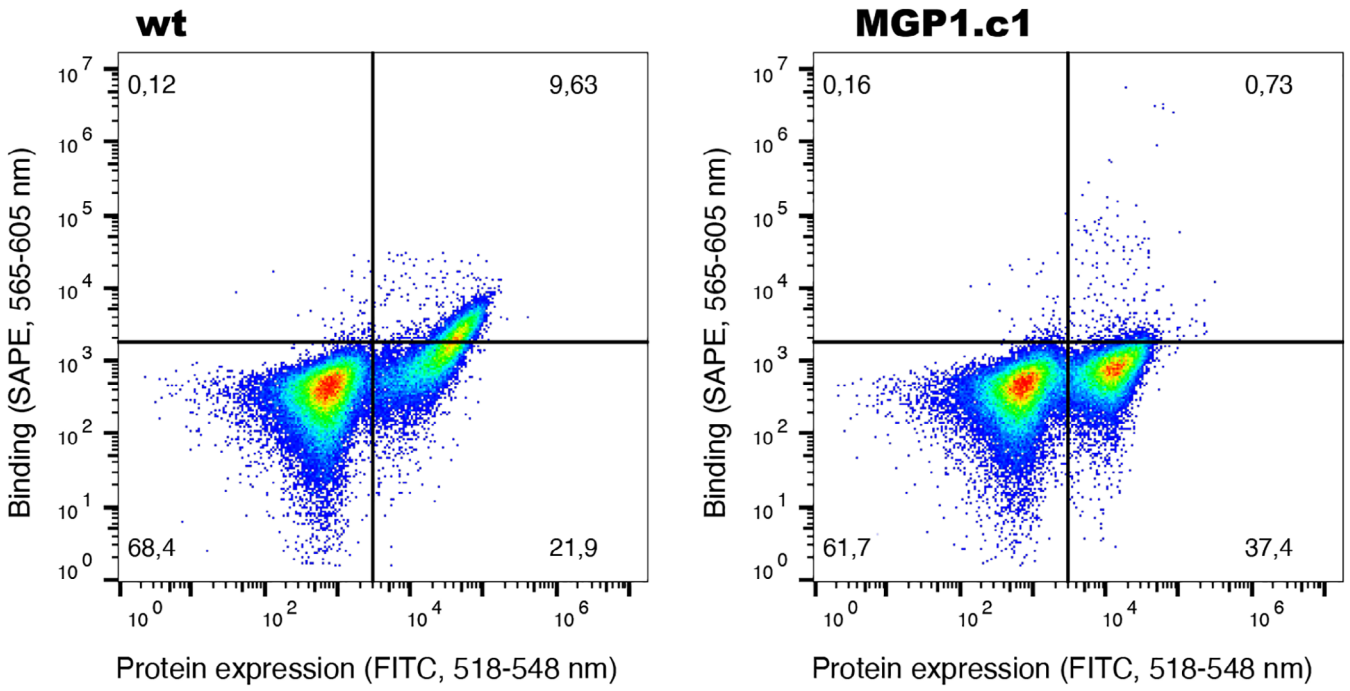

FIGURE 4 Binding of the glycan free MGP1 combined with the evolved mutations. By combining the selected mutations from MGP1 N95D/I126V/E130D/K170M variant with the alanine scanning mutations of Asn[137] and Asn[166], and the computationally favored N178D, resulted in the combined variant MGP1.c1 (N95D/I126V/E130D/N137A/N166A/K170M/N178D) that retained 40% binding to the target in comparison to the native binder. Assayed at 1 μM TfR for 60 000 gated singlet cells, in each quadrant the percentage of cells is indicated [Color figure can be viewed at wileyonlinelibrary.com]

affinity to TfR of ~7 nM.[44] Gold nanoparticles have also been coupled with anti TfR antibodies for brain delivery in mice.[18] Such binders may interact with other parts of the TfR than the surface targeted by Tf. Although, competition with H-Ft for binding at the apical domain may still interfere[45] as ferritin serum concentration is in the range of 20 to 600 nM[46] (~100 times lower than the transferrin concentration). Studying the MGP1-TfR interaction offers, apart from the insight of the virus binding mechanism, a way to bypass the competition with Tf for receptor-mediated endocytosis/transcytosis via TfR. Results from these studies may lead to engineering better interactions with the other domains of TfR not directly involved in interaction with Tf.

We have found several residues in MGP1 that are important for its interaction with TfR; mutagenesis of Ile[115] and Val[117] established these positions as hotspots, as in our system they abolish binding when mutated to alanine residues. The TfR residues Tyr[211], Asn[348], and Val[210] at the interface between MGP1 and the apical domain of TfR, have previously been characterized as determinants of host specificity for New World arenaviruses.[47,48] Especially Tyr[211] was found to be critical for viral (Machupo, Junín, and Guanarito) cell entry;[48] it makes extensive hydrophobic interactions with the identified Ile[115] and Val[117], but makes also an additional hydrogen bonds with Ser[113] in the glycoprotein as can be seen in TfR–MGP1 structure.[47] Calculations also identified Phe[226] (Figure 1A) as a potential hot spot residue which is supported by cell-based assays where Phe[226] did decrease the cell entry.[9] TfR Val[210] forms hydrophobic interactions mainly with MPG1 Phe[226] and Tyr[228] contributing to the hydrophobic interface formation. Thus, computational studies as well as YSD assay employed here established the Ile[115] and Val[117] as hot spot residues in addition to previously described Phe[226] residue.[9]

Glycans present on the surface of MGP1 have been shown to be important for solubility, and potentially functionality.[41] Three experimentally solved structures of MGP1 deposited in the PDB, one from insect cells[21] and two from Human Embryonic Kidney (HEK293T) cells,[41,49] have glycans present on the protein surface. The structure from insect cells and one of the HEK293T cells had glycans on all four *N*-glycosylation sites, while the remaining structure had only Asn[178] glycosylated. This further strengthens our finding that posttranslational modification of Asn[178] is functionally important and that it contributes upon modification to binding either by direct glycan interactions with the receptor or by inducing conformational changes in favor of binding. Our data overlaps with previously validated N178A mutation which showed weak TfR binding and abolished entry into HeLa and Vero cells.[9] In contrast to the glycosylated Asn[178] residue, our experiments suggest that the modified asparagine residues at the other positions are not required for binding. Our mutagenesis of individual glycosylated positions resulted in surface displayed protein as detected by anti-cmyc antibodies during YSD. A previous study had found that deglycosylation by endoglycosidase resulted in MGP1 precipitation, implying that glycans solubilize the protein.[41] Furthermore, their alanine knockouts are either functional or as in the case of Asn[95] there is an alternative mutation to aspartic acid that emerges during the selection process.

N95D increases the fluorescent signal of binding, and it seems that the mutation to the aspartic acid is responsible for the increased binding signal, not the loss of the glycan complex (Figure 5A). If there is a direct effect of losing the glycan behind the increased binding of N95D (the difference in the apparent binding constants of ~30 equals to ~2 kcal/mol), we would expect also an increased binding for N95A variant. The relative binding outcome of position 95 when changed from alanine to aspartate is thus even more striking. The alanine knockout may be less stable despite that it expresses on the yeast as monitored by the anti-cmyc tag. An alternative monitoring of the MGP1 expression with a protein that binds to it, but not overlapping with TfR interaction surface, would have been beneficial for assessing the correct folding during yeast display. Alternatively, the magnitude of the interaction may possibly be an effect of a structural rearrangement that favors complex formation, as the MGP1 consists of several loop fragments. Without the glycan present on Asp^{95}, a hydrophobic patch between Leu^{94} and the aromatic rings of Tyr^{228}, Phe^{98}, and His^{233} on MGP1 and Leu^{209} on TfR are exposed. Additionally, with the glycan missing, Arg^{208} of TfR and Ser^{97} of MGP1 are possible amino acids candidates for forming a salt bridge and hydrogen bond with Asp^{95}, respectively. However, Arg^{208} and Asp^{95} are, in the crystal structure, 9.6 Å apart (the closest nitrogen of Arg^{208} to the closest oxygen in Asp^{95}; Figure 5B). When combined with G230D mutation, Asp^{95} variant gained slightly improved binding. These residues form a locus that interacts with the beta-hairpin of Asp^{204}-Leu^{209} at the tip of the apical domain (Figure 5C). There seems to be a general flexibility in interactions in this region as the beta-hairpin is unstructured in the apo-TfR and also in the engineered stand-alone apical domain AP01[50] (PDB ID: **6y76**). In the AP01 structure, Arg^{208} side chain guanidium nitrogen atoms are as close as 6.5 Å from the side chain of the glycosylated Asn^{95} (overlayed onto the apical domain of the complexed receptor; PDB ID: **3kas**). The situation is reciprocated in the apo structure of MGP1[41] (PDB ID: **2wfo**) where the glycan attached to the Asn^{95} is at the interacting distance with the apical domain backbone residue Gly^{207} if we superimpose apo MGP1 structure on the corresponding subunit in the PDB ID: **3kas** complex. In summary, the above hairpin loop of the receptor (TfR positions 206-208) and the glycan of the position 95 in MGP1 overlap when apo structures are superimposed onto the complexed subunits. Together the combination of mutations, N95D and G230D, may lock onto the receptor more firmly without the original conformational change being necessary. One possible explanation for the virus to conserve glycosylation at position 95 is that N95D improves binding, but the glycosylation may protect the virus from host immune response or protease degradation. Alternatively, the apparent dissociation constant $K_d \approx 2$ μM indicates weak binding interaction between the glycoprotein and the receptor, which may be essential for viral dissociation as avidity may play a role due to high local density of MGP1 on virus particles.

It is important to note, that the YSD system is essentially different from in vitro measurements, and that the apparent K_d values that are derived should be viewed to some extent qualitatively. It has been found that the dissociation constants may differ when compared to in vitro measurements, for example, when determined by surface plasmon resonance.[24] One factor influencing the difference may be the local protein concentration on the surface of the yeast that is different when compared to the proteins in solution. Nevertheless, the situation on yeast may replicate the conditions found in other cell-based assays where they actually differ less than when compared with the in vitro data.[51] The yeast surface may thus be a more relevant environment corresponding to what is encountered in vivo. Second, the *N*-glycosylations are not being derived in the same way in mammalian cells when compared with yeast cells; yeast lacks the pathways needed for creating typically complicated mammalian cell glycosylation patterns, instead the yeast uses high-mannose type glycans, which at some instances are more sterically hindering than mammalian

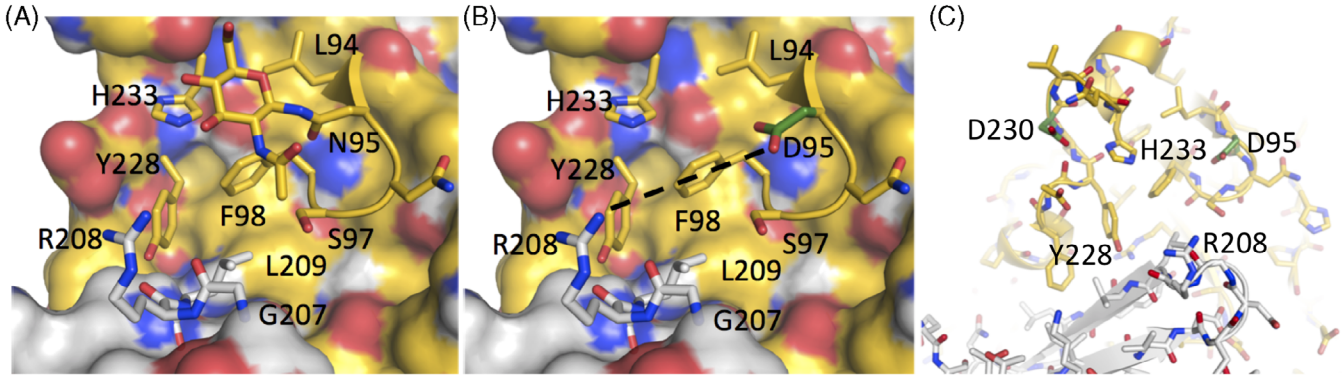

FIGURE 5 Structural analysis of the evolved MGP1.b1. Amino acid changes for MGP1.b1 (MGP1 N95D/G230D) are put into context of the structure by analyzing the complex of MGP1 with TfR (PDB ID: **3kas**, TfR in gray, MGP1 in yellow, and found mutations in green). A, Interactions of the MGP1 Asn^{95} *N*-glycan. A hydrophobic patch interacts with the glycan consisting of Leu^{94} and the aromatic side chains of Tyr^{228}, Phe^{98}, and His^{233} in MGP1, and receptor Leu^{209}. B, When mutated to aspartic acid, the hydrophobic center behind Asn^{95} is exposed, opening up for the possibility for TfR Arg^{208} and the backbone of Gly^{207} to reach Asp^{95} and Ser^{97} in the glycoprotein. C, N95D/G230D residues form interactions with the beta-hairpin of Asp^{204}-Leu^{209} at the tip of the apical domain, known to be unstructured in the apo-receptor. The motif forms basis for viral recognition of host species TfR [Color figure can be viewed at wileyonlinelibrary.com]

glycans.[52,53] This means that the N95D mutation may not necessarily give the same increase in binding affinity for in vitro produced protein from other hosts as it would depend on their glycosylation ability. Third, the control machinery that ensures for correct folding differs in yeast and mammalian cells. There is evidence that in some cases yeast cannot distinguish between misfolded and properly folded proteins during yeast display,[54] however, the apparent affinity changes and single point mutations supports that this is not the case for MGP1. To further strengthen our data, we have also carried out the competition assay that showed that 10 times more unlabeled TfR significantly reduced binding signal (by ~80%) to yeast surface expressed MGP1.b1. The competition assay demonstrates the lack of nonspecific binding, and supports directly forming interactions between virus glycoprotein and the receptor.

Based on the site-directed mutagenesis data and YSD/FACS selected variants we hypothesized that there should exist a variant with retained binding in which glycosylated positions are mutated and compensated by changes in other sites. We engineered such variant without glycan posttranslational modifications as it can be further improved on YSD for both binding and expression. The MGP1.c1 variant, that lacks the original glycosylation positions, but has the evolved mutations, retained 40% of the native MGP1 binding.

5 | CONCLUSION

In both the pursuit for finding therapeutic solutions for the NW arenaviruses and to get one step closer to using TfR as an entry point over the BBB, a greater understanding for the TfR-MGP1 interface is crucial. We have demonstrated that in the established YSD system, it is possible to assay and evolve variants of MGP1 to bind TfR with a higher affinity than for the native viral glycoprotein, and that MGP1 can still bind TfR without its *N*-glycosylation modifications. The demonstrated ability to optimize MGP1 and fine-tune interaction strength for binding allows for further study of TfR-mediated cell internalization and possibly for investigation of transport across the BBB.

ACKNOWLEDGMENTS

We thank Prof. Ingemar André at Lunds Universitet for the use of BioRad S3e and Jaromir Mikes at Science for Life Laboratory for initial FACS sorting. The computations were enabled by resources provided by SNIC at Lunarc (SNIC 2019/3-320).

CONFLICT OF INTERESTS

The authors declare no conflict of interest.

AUTHOR CONTRIBUTIONS

Dick J Sjöström and Sinisa Bjelic designed the study. Dick J Sjöström did the cloning, generated the MGP1 libraries, carried out the flow cytometry and FACS experiments. Sinisa Bjelic performed the computational modeling. Anneli Lundgren worked as a technician, carrying out initial experimental characterization. Dick J Sjöström, Scott J Garforth, and Sinisa Bjelic analyzed the data and wrote the manuscript.

ORCID

Sinisa Bjelic https://orcid.org/0000-0002-9300-614X

REFERENCES

1. Eckenroth BE, Steere AN, Chasteen ND, Everse SJ, Mason AB. How the binding of human transferrin primes the transferrin receptor potentiating iron release at endosomal pH. *Proc Natl Acad Sci U S A*. 2011;108(32):13089-13094.
2. Andrews NC, Schmidt PJ. Iron homeostasis. *Annu Rev Physiol*. 2007;69:69-85.
3. Li L, Fang CJ, Ryan JC, et al. Binding and uptake of H-ferritin are mediated by human transferrin receptor-1. *Proc Natl Acad Sci*. 2010;107(8):3505-3510.
4. Bennett MJ, Lebrón JA, Bjorkman PJ. Crystal structure of the hereditary haemochromatosis protein HFE complexed with transferrin receptor. *Nature*. 2000;403(6765):46-53.
5. Reuben A, Chung JW, Lapointe R, Santos MM. The hemochromatosis protein HFE 20 years later: an emerging role in antigen presentation and in the immune system. *Immun Inflamm Dis*. 2017;5(3):218-232.
6. Gruszczyk J, Huang RK, Chan LJ, et al. Cryo-EM structure of an essential *Plasmodium vivax* invasion complex. *Nature*. 2018;559(7712):135-139.
7. Radoshitzky SR, Kuhn JH, de Kok-Mercado F, Jahrling PB, Bavari S. Drug discovery technologies and strategies for Machupo virus and other New World arenaviruses. *Expert Opin Drug Discovery*. 2012;7(7):613-632.
8. Fedeli C, Moreno H, Kunz S. Novel insights into cell entry of emerging human pathogenic Arenaviruses. *J Mol Biol*. 2018;430(13):1839-1852.
9. Radoshitzky SR, Longobardi LE, Kuhn JH, et al. Machupo virus glycoprotein determinants for human transferrin receptor 1 binding and cell entry. *PLoS One*. 2011;6(7):e21398.
10. Radoshitzky SR, Abraham J, Spiropoulou CF, et al. Transferrin receptor 1 is a cellular receptor for New World haemorrhagic fever arenaviruses. *Nature*. 2007;446(7131):92-96.
11. Lebron JA, Bjorkman PJ. The transferrin receptor binding site on HFE, the class I MHC-related protein mutated in hereditary hemochromatosis. *J Mol Biol*. 1999;289(4):1109-1118.
12. West AP Jr, Giannetti AM, Herr AB, et al. Mutational analysis of the transferrin receptor reveals overlapping HFE and transferrin binding sites. *J Mol Biol*. 2001;313(2):385-397.
13. Giannetti AM, Bjorkman PJ. HFE and transferrin directly compete for transferrin receptor in solution and at the cell surface. *J Biol Chem*. 2004;279(24):25866-25875.
14. Cheng Y, Zak O, Aisen P, Harrison SC, Walz T. Structure of the human transferrin receptor-transferrin complex. *Cell*. 2004;116(4):565-576.
15. Testi C, Boffi A, Montemiglio LC. Structural analysis of the transferrin receptor multifaceted ligand(s) interface. *Biophys Chem*. 2019;254:106242.
16. Patel MM, Patel BM. Crossing the blood-brain barrier: recent advances in drug delivery to the brain. *CNS Drugs*. 2017;31(2):109-133.
17. Yu YJ, Atwal JK, Zhang Y, et al. Therapeutic bispecific antibodies cross the blood-brain barrier in nonhuman primates. *Sci Transl Med*. 2014;6(261):261ra154.
18. Johnsen KB, Bak M, Kempen PJ, et al. Antibody affinity and valency impact brain uptake of transferrin receptor-targeted gold nanoparticles. *Theranostics*. 2018;8(12):3416-3436.
19. Lee JH, Engler JA, Collawn JF, Moore BA. Receptor mediated uptake of peptides that bind the human transferrin receptor. *Eur J Biochem*. 2001;268(7):2004-2012.
20. Wiley DT, Webster P, Gale A, Davis ME. Transcytosis and brain uptake of transferrin-containing nanoparticles by tuning avidity to transferrin receptor. *Proc Natl Acad Sci U S A*. 2013;110(21):8662-8667.

21. Abraham J, Corbett KD, Farzan M, Choe H, Harrison SC. Structural basis for receptor recognition by New World hemorrhagic fever arenaviruses. *Nat Struct Mol Biol*. 2010;17(4):438-444.
22. Boder ET, Wittrup KD. Yeast surface display for screening combinatorial polypeptide libraries. *Nat Biotechnol*. 1997;15(6):553-557.
23. Gai SA, Wittrup KD. Yeast surface display for protein engineering and characterization. *Curr Opin Struct Biol*. 2007;17(4):467-473.
24. Fleishman SJ, Whitehead TA, Ekiert DC, et al. Computational design of proteins targeting the conserved stem region of influenza hemagglutinin. *Science*. 2011;332(6031):816-821.
25. Singh MV, Weil PA. A method for plasmid purification directly from yeast. *Anal Biochem*. 2002;307(1):13-17.
26. Benatuil L, Perez JM, Belk J, Hsieh CM. An improved yeast transformation method for the generation of very large human antibody libraries. *Protein Eng Des Sel*. 2010;23(4):155-159.
27. Chao G, Lau WL, Hackel BJ, Sazinsky SL, Lippow SM, Wittrup KD. Isolating and engineering human antibodies using yeast surface display. *Nat Protoc*. 2006;1(2):755-768.
28. Pham PL, Kamen A, Durocher Y. Large-scale transfection of mammalian cells for the fast production of recombinant protein. *Mol Biotechnol*. 2006;34(2):225-237.
29. FlowJo™ Software Version 10.5.0.[computer program]. Ashland, OR: Becton, Dickinson and Company 2019.
30. R: A language and environment for statistical computing. [computer program]. R Foundation for Statistical Computing, Vienna, Austria. https://www.R-project.org/2019.
31. Ritz C, Baty F, Streibig JC, Gerhard D. Dose-response analysis using R. *PLoS One*. 2015;10(12):e0146021.
32. Fleishman SJ, Leaver-Fay A, Corn JE, et al. RosettaScripts: a scripting language interface to the Rosetta macromolecular modeling suite. *PLoS One*. 2011;6(6):e20161.
33. Leaver-Fay A, Tyka M, Lewis SM, et al. ROSETTA3: an object-oriented software suite for the simulation and design of macromolecules. *Methods Enzymol*. 2011;487:545-574.
34. Huang PS, Ban YE, Richter F, et al. RosettaRemodel: a generalized framework for flexible backbone protein design. *PLoS One*. 2011;6(8):e24109.
35. Alford RF, Leaver-Fay A, Jeliazkov JR, et al. The Rosetta all-atom energy function for macromolecular modeling and design. *J Chem Theory Comput*. 2017;13(6):3031-3048.
36. Schrodinger, LLC. The PyMOL Molecular Graphics System, Version 2.3.4. In: 2015.
37. Altschul SF, Madden TL, Schäffer AA, et al. Gapped BLAST and PSI-BLAST: a new generation of protein database search programs. *Nucleic Acids Res*. 1997;25(17):3389-3402.
38. Altschul SF, Wootton JC, Gertz EM, et al. Protein database searches using compositionally adjusted substitution matrices. *FEBS J*. 2005;272(20):5101-5109.
39. Schäffer AA, Aravind L, Madden TL, et al. Improving the accuracy of PSI-BLAST protein database searches with composition-based statistics and other refinements. *Nucleic Acids Res*. 2001;29(14):2994-3005.
40. Thomsen MC, Nielsen M. Seq2Logo: a method for construction and visualization of amino acid binding motifs and sequence profiles including sequence weighting, pseudo counts and two-sided representation of amino acid enrichment and depletion. *Nucleic Acids Res*. 2012;40:W281-W287.
41. Bowden TA, Crispin M, Graham SC, et al. Unusual molecular architecture of the machupo virus attachment glycoprotein. *J Virol*. 2009;83(16):8259-8265.
42. Hultqvist G, Syvänen S, Fang XT, Lannfelt L, Sehlin D. Bivalent brain shuttle increases antibody uptake by monovalent binding to the transferrin receptor. *Theranostics*. 2017;7(2):308-318.
43. Wessling-Resnick M. Crossing the iron gate: why and how transferrin receptors mediate viral entry. *Annu Rev Nutr*. 2018;38(1):431-458.
44. Dautry-Varsat A, Ciechanover A, Lodish HF. pH and the recycling of transferrin during receptor-mediated endocytosis. *Proc Natl Acad Sci U S A*. 1983;80(8):2258-2262.
45. Montemiglio LC, Testi C, Ceci P, et al. Cryo-EM structure of the human ferritin-transferrin receptor 1 complex. *Nat Commun*. 2019;10(1):1121.
46. Wang W, Knovich MA, Coffman LG, Torti FM, Torti SV. Serum ferritin: past, present and future. *Biochim Biophys Acta*. 2010;1800(8):760-769.
47. Abraham J, Kwong JA, Albariño CG, et al. Host-species transferrin receptor 1 orthologs are cellular receptors for nonpathogenic new world clade B arenaviruses. *PLoS Pathog*. 2009;5(4):e1000358.
48. Radoshitzky SR, Kuhn JH, Spiropoulou CF, et al. Receptor determinants of zoonotic transmission of New World hemorrhagic fever arenaviruses. *Proc Natl Acad Sci U S A*. 2008;105(7):2664-2669.
49. Clark LE, Mahmutovic S, Raymond DD, et al. Vaccine-elicited receptor-binding site antibodies neutralize two New World hemorrhagic fever arenaviruses. *Nat Commun*. 2018;9(1):1884.
50. Sjöström DJ, Berger SA, Oberdorfer G, Bjelic S. Computational backbone design enables soluble engineering of transferrin receptor apical domain. *Proteins*. 2020:1-9. https://doi.org/10.1002/prot.25974.
51. Cochran JR, Kim YS, Olsen MJ, Bhandari R, Wittrup KD. Domain-level antibody epitope mapping through yeast surface display of epidermal growth factor receptor fragments. *J Immunol Methods*. 2004;287(1–2):147-158.
52. Kowalsky CA, Whitehead TA. Determination of binding affinity upon mutation for type I dockerin-cohesin complexes from clostridium thermocellum and clostridium cellulolyticum using deep sequencing. *Proteins*. 2016;84(12):1914-1928.
53. Wildt S, Gerngross TU. The humanization of N-glycosylation pathways in yeast. *Nat Rev Microbiol*. 2005;3(2):119-128.
54. Medina-Cucurella AV, Zhu Y, Bowen SJ, Bergeron LM, Whitehead TA. Pro region engineering of nerve growth factor by deep mutational scanning enables a yeast platform for conformational epitope mapping of anti-NGF monoclonal antibodies. *Biotechnol Bioeng*. 2018;115(8):1925-1937.

SUPPORTING INFORMATION

Additional supporting information may be found online in the Supporting Information section at the end of this article.

How to cite this article: Sjöström DJ, Lundgren A, Garforth SJ, Bjelic S. Tuning the binding interface between Machupo virus glycoprotein and human transferrin receptor. *Proteins*. 2021;89:311–321. https://doi.org/10.1002/prot.26016